ACS OMEGA

Open Access

http://pubs.acs.org/journal/acsodf

Article

Protective Mechanisms of Siloxane-Modified Epoxy Novolac Coatings at High-Pressure, High-Temperature Conditions

Narayanan Rajagopalan,* Mads Olsen, Toke Skaarup Larsen, Tine Jensen Fjælberg, Claus Erik Weinell, and Søren Kiil*

Cite This: *ACS Omega* 2024, 9, 30675−30684

Read Online

ACCESS | Metrics & More | Article Recommendations | Supporting Information

ABSTRACT: In the context of high-pressure, high-temperature (HPHT) conditions resembling those in the oil and gas industry, the performance of epoxy-siloxane hybrid coatings is investigated. Neat amine-cured epoxy novolac (EN) coatings exhibit drawbacks under these conditions, including softening upon exposure to hydrocarbons, leading to underfilm corrosion triggered by CO_2 gas and seawater ion diffusion. To address these issues, two hybrid coatings, long-chain epoxy-terminated polydimethylsiloxane-modified EN (EN-EPDMS) and short-chain 3-glycidyloxypropyltrimethoxysilane-modified EN (EN-GPTMS), are assessed in HPHT environments. Both hybrids mitigate drawbacks observed in neat EN, with EN-GPTMS completely eliminating them due to the chemical inertness of inorganic siloxane networks. While EN-EPDMS exhibits a higher glass transition temperature than EN-GPTMS, it is susceptible to rapid gas decompression due to its lengthy and flexible siloxane backbone, resulting in unburst blisters. Conversely, EN-GPTMS demonstrates superior performance in HPHT environments, highlighting its potential for effective corrosion protection in harsh conditions encountered by the oil and gas industry.

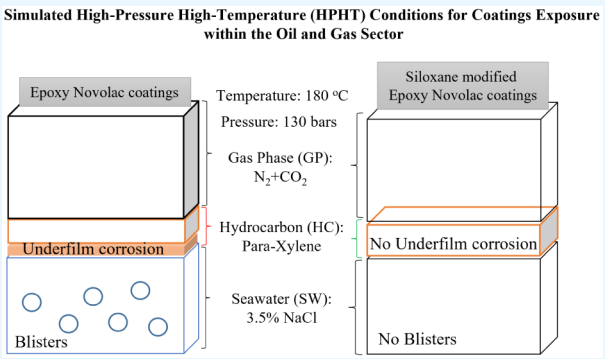

1. INTRODUCTION

The vast utilization of reservoirs has pushed many of the existing oil and gas fields toward depletion. This forces the industry to go for deeper wells and abnormal geological structures, known as high-pressure and high-temperature (HPHT) conditions, and the most common HPHT definition is when the environment exceeds a pressure of 690 bar (10,000 psi) and/or a temperature of 149 °C (300 °F).[1,2] These extreme conditions, however, result in new corrosion challenges, such as substrate longevity and durability, in particular, for downstream-buried pipelines.

The coexistence of different gases and chemicals, such as H_2S and CO_2, a mixture of hydrocarbon fluids, and seawater,[3−6] at high pressures and high temperatures intensifies the extremity of HPHT, thereby accelerating the corrosion processes. Normally, high-performance anticorrosive epoxy coatings protect the inside of wells, storage tanks, and pipelines. Due to their strong metal adhesion, high chemical resistance, and suitable processing characteristics, two-component epoxies are widely used as protective coatings in the heavy-duty industry.[7,8] However, recent studies on degradation pathways for an amine-cured epoxy novolac (EN) coating at HPHT confirmed an initial hydrocarbon interaction (softening), which significantly lowered the network T_g and accelerated the diffusion of CO_2 gas and seawater ions into the EN network, subsequently triggering underfilm corrosion.[9,10] To sustain the extremity of HPHT conditions, these unfavorable attributes of EN coatings demonstrate a need for improvement. For the past two decades, silicon derivatives have been used in coatings as modification (or coupling) agents and cobinders (cross-linkers) to improve the chemical resistance, solvent resistance, thermal stability, and flexibility of the cured coating system.[11−13] Due to the polyfunctional siloxane (Si−O) bond present in the backbone chains of a silicon derivative, silanes and silicones have gained immense commercial importance. The strong chemical bonding inherent within the siloxane networks and the associated thermal stability promote inertness against chemical attack. This nominates silanes and silicones as qualified candidates for the development of epoxy-siloxane hybrid coatings under HPHT conditions.

A silicon derivative, when used as an adhesion promoter, commonly takes the form of a silane, represented as $(AO)_3SiB$, where AO is a hydrolyzable alkoxy group and B is an organofunctional group. The silane utilized in this study is 3-

Received: March 28, 2024
Revised: June 20, 2024
Accepted: June 21, 2024
Published: July 7, 2024

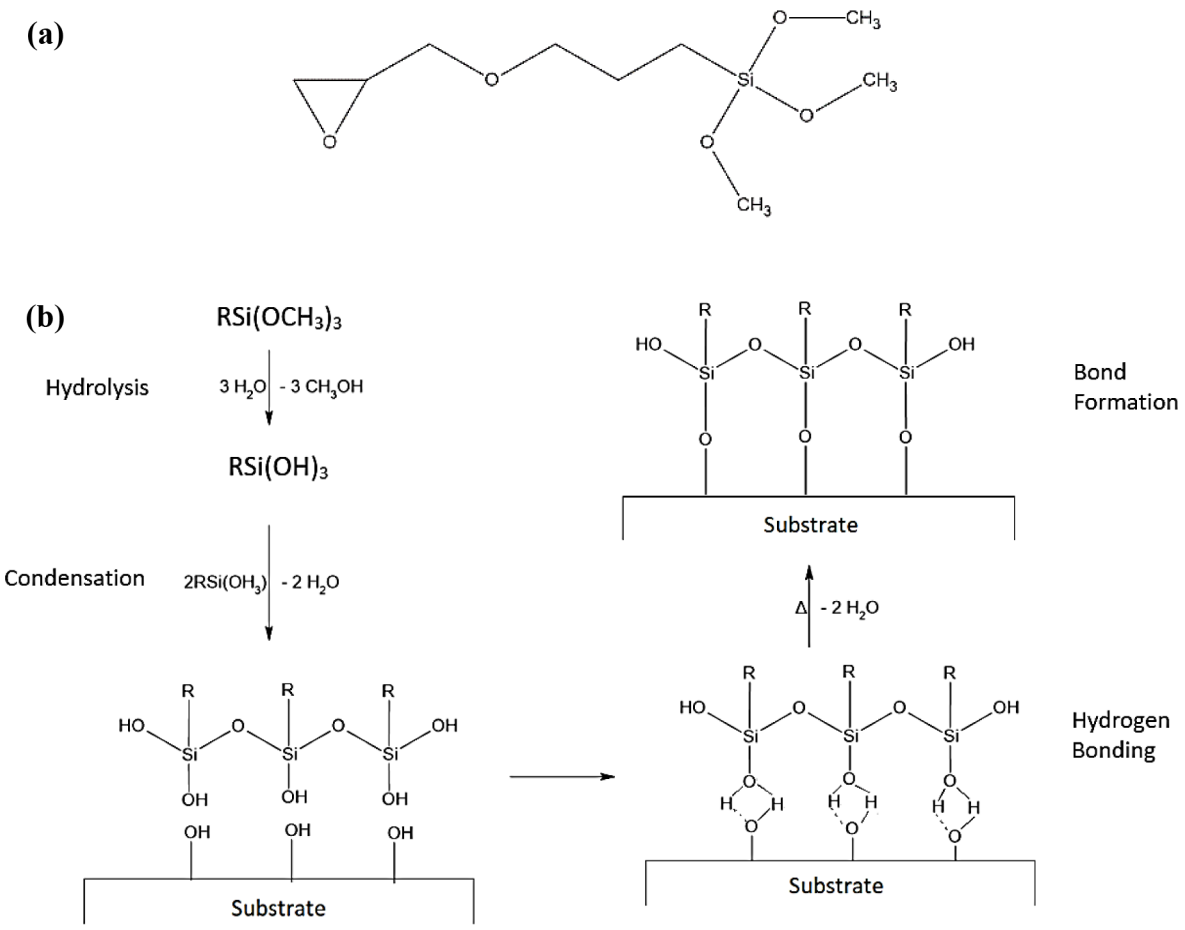

Figure 1. (a) Molecular structure of GPTMS and (b) schematic illustration of Si−O bonding to the metal substrate when used as an adhesion promoter.

glycidyloxypropyltrimethoxysilane (GPTMS), with the molecular structure shown in Figure 1a. Due to condensation reactions between silanols (Si−OH, the hydrolysis product of the alkoxy group) and the metal (substrate) hydroxyls (Me−OH), silanes act as adhesion promoters, forming siloxane bonds (Si−O−Si) and metal−siloxane bonds (Me−O−Si), as shown in Figure 1b. The electropositive atomic structure of silicon generates a high dipole moment for the silanol groups, thereby improving the formation of hydrogen bonds.[12]

Silicones (polysiloxanes), on the other hand, consist of higher-molecular-weight siloxanes with either a hydroxyl terminal group or a terminal epoxy functionalization. Silicones are polymeric with repeating units [−Si(R)$_2$−O−] and correspond to polydialkylsiloxanes, with a structure, where R commonly represents methyl or phenyl groups.[14] Epoxy-terminated polydimethylsiloxane (EPDMS), shown in Figure 2, was selected as the long-chain silicone resin for the present study.

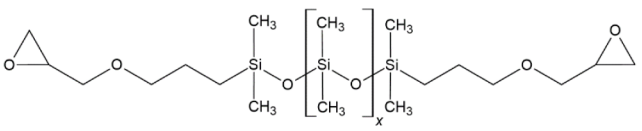

Figure 2. Molecular structure of EPDMS with repeating dimethylsiloxane groups and epoxy functional terminated groups.

Previous studies extensively examined the anticorrosion properties of silicone derivatives and their structure−property relationships.[15−25] However, limited research is reported on exploring the synergistic effects of hydrocarbon interactions and CO_2 gas and seawater ion diffusion into epoxy-siloxane hybrids under high-pressure and high-temperature (HPHT) conditions. Silicone derivatives, characterized by structural aspects, high-thermal stability, hydrophobicity, and chemical resistance, provide insights into the interactions of epoxy-siloxane hybrids at HPHT.

The unique properties of organic−inorganic silicon derivatives originate from the extensive delocalization of sigma electrons along the silicone backbone, enhancing stability.[15] Factors such as polymer molecular weight, substituent nature, and molecular conformation further modulate these properties.[15] The high Si−O bond energy, close similarity to an ionic bond, and exceptional thermal and thermo-oxidative resistance contribute to the stability of silicones in extreme conditions.[16,17] In terms of heat resistance, research has shown that silicone rubber performed superior to organic rubbers. No alterations were observed at 150 °C and withstanding 10,000 consecutive hours, even at a service temperature of 200 °C.[15]

In terms of gas diffusion properties, the polymer structure (i.e., degree of crystallinity, thermal and mechanical properties), penetrant size and nature, temperature, and pressure significantly influence gas permeability.[18] Concerning the water penetration, silicone rubber exhibits minimal water absorption (only 1%) even after prolonged exposure without compromis-

https://doi.org/10.1021/acsomega.4c02986
ACS Omega 2024, 9, 30675−30684

ing mechanical or electrical properties.[19] Incorporating silanes into epoxy novolac networks enhances hydrophobicity and reduces water penetration.[20] Although water still penetrated the structures, the water fraction within the silane-epoxy network, compared to the neat epoxy novolac, was crucially reduced.

Another study by Mazurek[21] relevant to HPHT, confirmed silicone rubber's outstanding oil resistance at high temperatures compared to organic rubbers.[21] Southwart[22] reported that silicone rubber's swelling behavior in organic compounds is reversible, unlike most organic rubbers, which decompose or dissolve upon solvent removal.

In essence, the postulation leading to the incorporation of silanes and silicones in the epoxy network arises from their multifunctional properties. The present work aims at understanding the fundamental roles of a short-chain silane (GPTMS) and a long-chain silicone (EPDMS) in extending the range of physical and chemical properties of conventional amine-cured epoxy novolac (EN) coatings for HPHT applications. Assessing the interaction of the three phases with the two hybrid coatings at HPHT is the primary focus. Both EN-GPTMS and EN-EPDMS hybrid coatings consist of only resins, curing agents, and silicon derivatives. The formulations are devoid of any pigments, fillers, or additives, allowing for a more accurate interpretation of the interactions. Additionally, the findings provide relevance for other extreme applications such as heat exchanger tubes, combustion chambers, power-to-X conversion technologies, and CO_2-resistant pipeline coatings for the next-generation carbon capture and storage (CCS) domain.[23−25]

2. EXPERIMENTAL SECTION

2.1. Coating Formulation and Application. In the present study, to formulate an amine-cured epoxy novolac (EN) coating, DEN 438-X80 (epoxy novolac) with a functionality (f) = 3.6 was selected as the resin base, and two polyamines, bisphenol A adducted *m*-xylylenediamine (MXDA) and bisphenol A adducted 3-diethylaminopropylamine (DEAPA), were selected as the curing agents. The stoichiometric ratio (0.3−0.6) between the epoxy and amine functional groups for EN and the curing conditions were according to the commercial grade coatings existing for HPHT applications. The base components, consisting of epoxy novolac resin and the respective silane (GPTMS) and siloxane (EPDMS), were blended using a high-speed disperser (DISPERMAT CV3-PLUS, VMA-Getzmann GmbH, Germany) at approximately 5000 rpm for 15 min. Following this, the curing agents, the MXDA adduct and DEAPA adduct, were incorporated into the base mixture at a stoichiometric ratio (SR) ranging from 0.3 to 0.6, ensuring an excess of epoxy. The concentration of GPTMS in the EN-GPTMS formulation was selected in the interval from 0.5 to 4 wt %. Similarly, the EN-EPDMS formulation was prepared by replacing short-chained GPTMS with long-chained EPDMS (0.5 to 4 wt %). Using a smooth natural bristle paintbrush of width 50 mm, both hybrid coatings were applied to steel panels with dimensions of 5 mm × 70 mm × 120 mm. A magnetic gauge instrument, Elcometer model 355 Top, was used to measure the first coat thickness (75 ± 10 μm), and after the second coat, a total DFT of 150 ± 25 μm was obtained. The recoating interval between the first and second coats was 12 h, and the coatings were applied on both sides, also covering the edges of the panel. After the coating application, the samples were cured at room temperature for 5 days, followed by postcuring at 120 °C for 3 h. Due to the presence of unreacted epoxy groups after room temperature curing, the elevated temperature (postcuring) enhanced the cross-linking further.

2.2. HPHT Reactor Setup. To simulate HPHT conditions, an enclosed batch reactor (0.97 L autoclave chamber), procured from Parr instruments, was utilized.[9,10] A mixture of N_2 and CO_2 as the gas phase, *para*-xylene (200 mL) as the hydrocarbon phase, and 3.5% NaCl solution (400 mL) as the artificial seawater phase constituted the HPHT phases inside the reactor chamber as depicted in Figure 3. The completely cured EN-GPTMS and EN-EPDMS panels were placed vertically inside the chamber. According to the HPHT definitions, if any of the two parameters (pressure or temperature) are accomplished, then the conditions fall under the HPHT category. Even though a pressure rating of 690 bar is emphasized in the HPHT definitions,[1,2] the actual pressure at the upstream oil and gas applications (where coating technology plays a more prominent role) differs from ambient to 150 bar.[26] After closing the chamber, the initial procedure involved removing oxygen by purging the chamber with high-pressure N_2 gas for 20 min. Subsequently, a specific mixture of N_2 and CO_2 was introduced into the chamber to attain a pressure of 100 bar at room temperature. The chamber, pressurized as such, was then heated to 180 °C using a Calrod heater, with a heating rate of 5 °C/min, resulting in a pressure increase to 130 bar. For all experiments, a benchmark pressure of 130 bar and a temperature of 180 °C were maintained for an exposure time of 12 h.

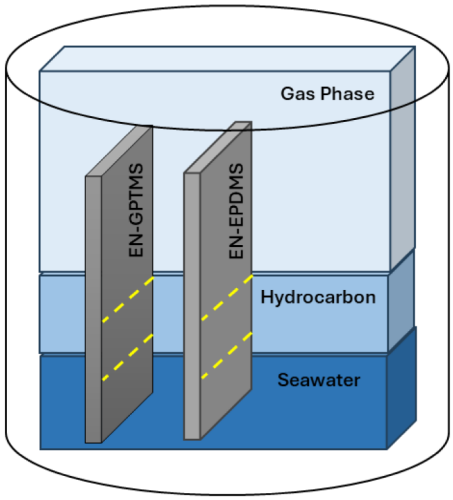

Figure 3. A schematic depiction of the autoclave chamber illustrating the various phases (gas, hydrocarbon, and artificial seawater phases) constituting the high-pressure, high-temperature (HPHT) condition, along with vertically positioned EN-GPTMS and EN-EPDMS coated panels within the batch reactor. The dotted yellow lines represent the HPHT phase boundaries.

2.3. Characterization Techniques. *2.3.1. Digital Microscopy.* The surface morphology of EN-EPDMS and EN-GPTMS specimens before and after HPHT was analyzed with a digital microscope (VHX-6000, manufacturer Keyence, Belgium) with the lens VH-Z20T, capable of magnifying up to 200 times.

2.3.2. Scanning Electron Microscopy. To detect the surface morphological changes before and after HPHT exposure, a

https://doi.org/10.1021/acsomega.4c02986
ACS Omega 2024, 9, 30675−30684

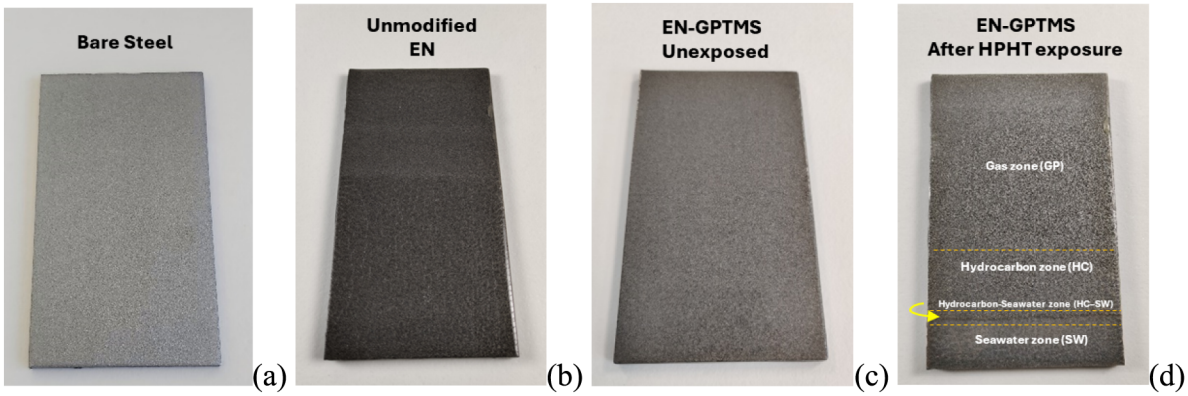

Figure 4. (a) Bare steel surface. (b) Unmodified EN coating. (c) The silane-modified epoxy novolac (EN-GPTMS) hybrid coating before HPHT exposure. (d) After the HPHT exposure showing no major defects. The dotted yellow lines in (d) represent the HPHT phase boundaries.

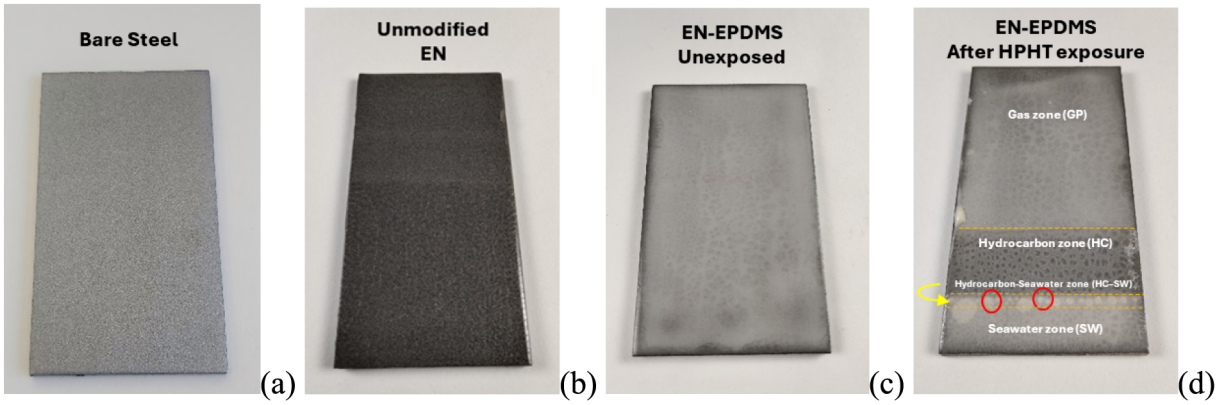

Figure 5. (a) Bare steel surface. (b) Unmodified EN coating. (c) Epoxy-terminated silicone-modified epoxy novolac (EN-EPDMS) hybrid coating before HPHT exposure and (d) after HPHT exposure, showing three resultant zones with blister formation in the HC−SW subzone (marked with red circles). The dotted yellow lines in (d) represent the HPHT phase boundaries.

scanning electron microscope (SEM) (Prisma ESEM, manufacturer Thermofisher Scientific, Denmark) operated at an accelerating voltage of 20 kV was utilized. The SEM accessorized with energy-dispersive X-ray (EDX) further defined the defects and qualitatively identified the presence of any heterogeneities at the surface. To prepare the samples for SEM imaging of the coating−steel interface in the hydrocarbon−seawater (HC−SW) region, steel samples were first identified and marked for cutting. Using a cutting machine, the samples were precisely cut along the designated line representing the HC−SW region. Subsequently, the exposed cross-sectional surfaces were meticulously polished to achieve a smooth and flat surface suitable for imaging. After polishing, the samples were thoroughly cleaned to remove any debris or contaminants. To enhance the surface conductivity for SEM analysis, a thin layer of silver was then sputtered onto the polished surfaces. Finally, the prepared samples were placed in the SEM chamber for imaging, allowing for detailed observation and analysis of the coating−steel interface morphology and structure in the HC−SW region.

2.3.3. Differential Scanning Calorimetry (DSC). Using a "Discovery" Model DSC apparatus (manufacturer TA Instruments, Denmark), DSC studies were performed. About 10 mg of both the hybrid coatings (before and after HPHT exposure) in powder form (scrapped off from the coating surface) were placed in closed aluminum DSC pans. Using a clean and sharp tool, a sufficient amount of coating (10 mg) was uniformly scraped off from the HC−SW region, ensuring thorough coverage. To account for potential variations, the scraping process was repeated at least three times in different areas from each of the different regions developed after HPHT exposure. The spectra were recorded from room temperature to 350 °C at a heating rate of 10 °C/min. To monitor the change in average T_g values of EN-EPDMS and EN-GPTMS coatings before and after HPHT exposures, dynamic experiments utilizing the standard heat−cool−reheat cycles were executed. The T_g value was evaluated from the second heat cycle. DSC measurements were conducted at two different areas of each zone for both hybrid coatings. It should be stated that there was only a negligible difference (±1.5 °C) in the T_g value when the sample was measured as a free film (solid) and as powder (scrapped off).

3. RESULTS AND DISCUSSIONS

The following findings and results originate from the surface analysis of EN-GPTMS and EN-EPDMS hybrid coatings, before and after HPHT exposure, that include visual, optical, and SEM analyses coupled with elemental mapping of the exposed surface. Furthermore, a detailed understanding of the degradation pathway for both hybrid coatings, after the HPHT exposure, is achieved by measuring the change in the average T_g at each of the three zones.

3.1. Optical Analysis before and after HPHT Exposure. *3.1.1. Visual Inspection.* The fully cured EN-

https://doi.org/10.1021/acsomega.4c02986
ACS Omega 2024, 9, 30675−30684

GPTMS coating (Figure 4c) before exposure showed a homogeneous and transparent film, yet exhibited a mild surface incompatibility, resulting in microphase separations. After HPHT exposure, the EN-GPTMS panel remained unaffected at all three exposed zones, as shown in Figure 4d. Neither the gas phase-exposed zone (GP) nor the hydrocarbon-exposed zone (HC) showed any visual surface imperfections. Additionally, due to salt depositions at the surface, the seawater-exposed zone (SW) remained intact with a mild, white discoloration.

Due to the longer chain length and higher molecular weight of EPDMS compared to GPTMS, the microphase separation was even more significant for the fully cured unexposed EN-EPDMS coating (Figure 5c). The EN-EPDMS coating, after HPHT exposure, led to three distinct zones, resulting from the three HPHT phases, as shown in Figure 5d. The gas-exposed zone and the hydrocarbon-exposed zone, except for a mild discoloration at the hydrocarbon-exposed zone, showed no defects. On the other hand, blister formations (marked with red circles in Figure 5d) next to the hydrocarbon−seawater interface (HC−SW) were significant. The seawater-exposed zone remained intact and unaffected.

3.1.2. Digital Micrographs. Digital microscopy (DM) attained a higher depth of visualization for the examination of the surface characteristic changes at the resultant zones after HPHT exposure. As seen in Figure 6b−d, all three zones for

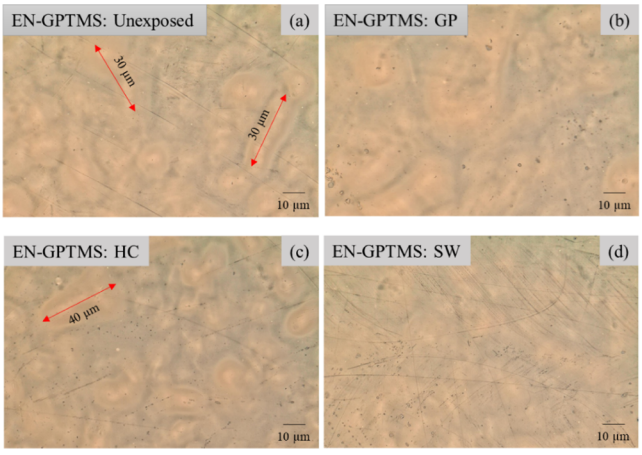

Figure 6. Digital microscope images of (a) the unexposed EN-GPTMS and (b), (c), and (d) showing the three relevant zones formed on EN-GPTMS after HPHT exposure with microphase separations marked by double-sided red arrows. (b) GP − gas phase, (c) HC − hydrocarbon phase, and (d) SW − seawater phase.

EN-GPTSMS, after exposure, displayed no major surface defects. Furthermore, the microphase separations that were present at the coating surface prior to exposure remained unchanged for all three resultant zones.

In the case of EN-EPDMS, a similar trend of surface characteristics was observed. The three resultant zones after HPHT exposure (Figure 7b−d) were intact and free from any surface defects. However, the microphase separations for EN-EPDMS (Figure 7a) were observed to be larger (80−100 μm) than EN-GPTMS (30 to 40 μm) as seen in Figure 6a. Moreover, the DM analysis after HPHT exposure suggested that the microphase separations for both EN-GPTMS and EN-EPDMS were merely a surface incompatibility and had no influence on the corrosion resistance attributes at HPHT. In

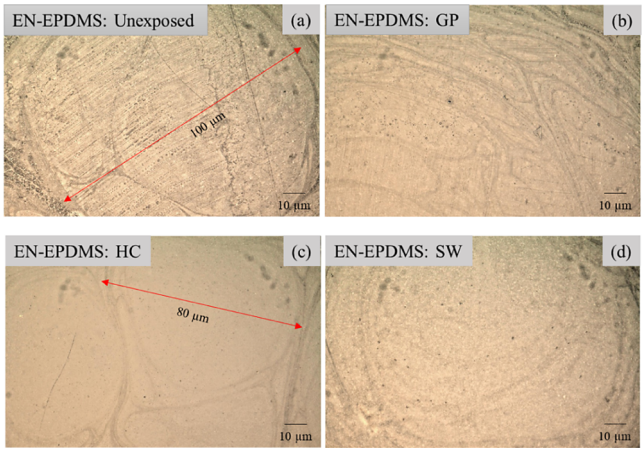

Figure 7. Digital micrographs of (a) the unexposed EN-EPDMS and (b), (c), and (d) representing the microphase separated surface of the three resultant zones on the EN-EPDMS coating after HPHT exposure, confirming the absence of surface degradation.

the literature, owing to the incompatibility between the epoxy resin and the silicon derivatives,[27] microphase separation is anticipated.

3.1.3. SEM−EDX Analyses. To substantiate the DM images and obtain an understanding of the EN-GPTMS and EN-EPDMS surfaces, SEM analysis on their three resultant HPHT zones was conducted.

As seen from Figure 8b−d, the three resultant zones for EN-GPTMS after HPHT exposure showed no surface imperfec-

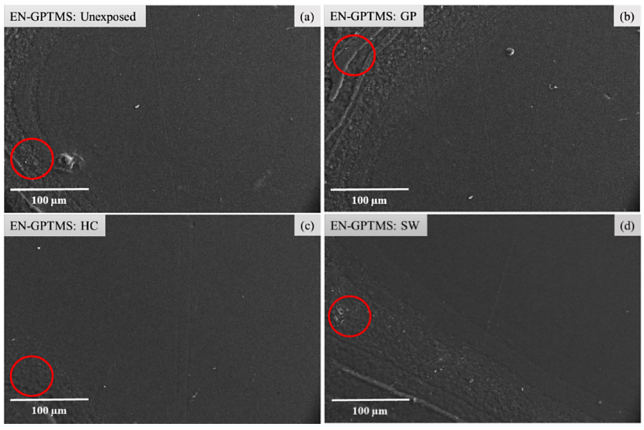

Figure 8. (a) SEM micrograph of the unexposed EN-GPTMS coating. (b), (c), and (d) show the surface morphology of gas (GP), hydrocarbon (HC), and seawater (SW) zones, respectively, after HPHT exposure. The microphase separation (marked with red circles), also present in the unexposed sample, remains unchanged at all three HPHT zones.

tions. SEM analysis was able to detail the morphology of the microphase separations (marked with red circles) present on the exposed sample. The microphase boundary in this case was structurally insignificant and played no role in accelerating any kind of corrosion degradation.

Similarly, the SEM micrographs (Figure 9b−d) of the three resultant zones on EN-EPDMS show a defect-free surface, analogous to EN-GPTMS. However, a more significant morphology for the microphase separations is seen. The morphology of the microphase boundaries comprised protrud-

https://doi.org/10.1021/acsomega.4c02986
ACS Omega 2024, 9, 30675−30684

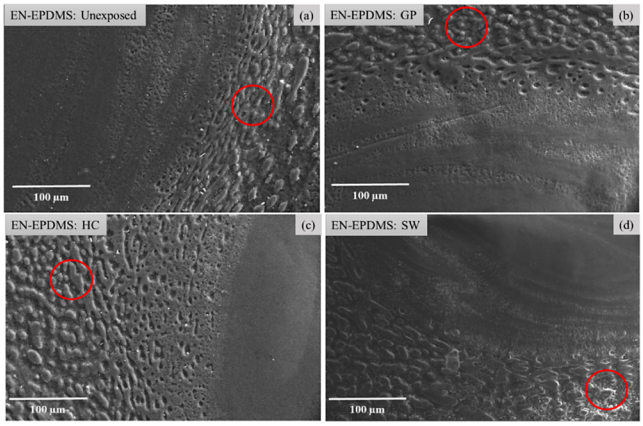

Figure 9. EN-EPDMS hybrid coating showing the SEM micrographs of (a) the unexposed EN-EPDMS. Surface morphology of the three resultant zones (b), (c), and (d) on EN-EPDMS on exposure to HPHT. The microphase separation (marked with red circles) observed for EN-EPDMS is more significant and protruding compared to EN-GPTMS.

ing island structures of size ranging from 10 to 20 μm (area marked with red circles). All three zones of EN-EPDMS complemented the DM observations and confirmed that no degradation has occurred on the coating surface or the microphase boundaries.

The SEM cross-sectional micrographs for both EN-GPTMS and EN-EPDMS coatings (Figure 10b,c) further confirmed that the metal coating interface, which was identified as the source of iron oxide (underfilm corrosion) for a neat organic EN coating, remained entirely defect-free. This observation aligns with the evidence, indicating the absence of iron oxide

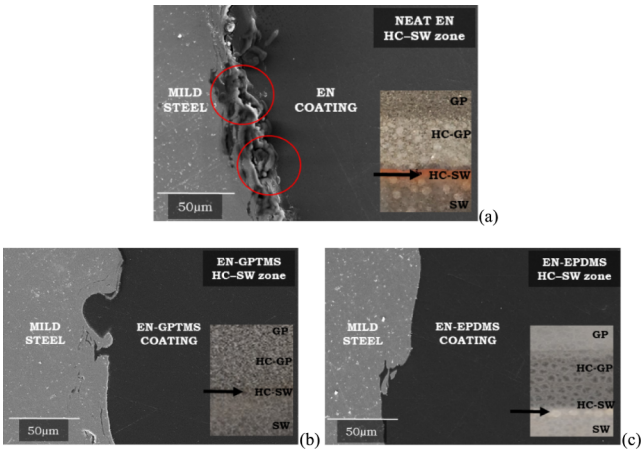

Figure 10. (a) SEM cross-sectional micrograph of neat EN coating after HPHT exposure at its hydrocarbon–seawater subzone (HC–SW), showing corrosion products (area marked with red circles) at its steel-coating interface. (Reprinted with permission from Rajagopalan, N., Weinell, C. E., Dam-Johansen, K., & Kiil, S. Influence of CO2 at HPHT Conditions on the Properties and Failures of an Amine-Cured Epoxy Novolac Coating. *Ind. Eng. Chem. Res.* 2021, *60*(41), 14768–14778. Copyright 2021 American Chemical Society.) Similarly, (b) and (c) are SEM cross-sectional images of EN-GPTMS and EN-EPDMS, respectively, at their HC–SW subzones after HPHT exposure. In the case of (b) and (c), the steel-coating interface was completely defect-free, and no corrosion products were observed. The black arrow in (a), (b), and (c) represents the area where the cross-sectional imaging was performed.

deposition at the hydrocarbon–seawater (HC–SW) interface for both EN-GPTMS (Figure 4d) and EN-EPDMS (Figure 5d).

It is evident from the optical micrographs and SEM analysis that the epoxy-siloxane hybrid networks sustained the HPHT exposure with no substantial surface defects or change in its surface morphology.

3.2. DSC Analysis. Using DSC analysis (i.e., DSC thermographs for all samples, before and after HPHT exposure, provided as Figures S1 and S2), the effect of HPHT conditions on the cross-linking attributes of both EN-GPTMS and EN-EPDMS hybrid coatings was investigated. The primary focus was to evaluate the average T_g value before and after HPHT exposure for both hybrids as summarized in Table 1. The initial average T_g value for EN-GPTMS and EN-EPDMS before HPHT exposure was measured to be 157 ± 3 °C and 158 ± 2 °C, respectively.

Table 1. Average Glass Transition Temperatures (T_g) for the EN-GPTMS and EN-EPDMS Coatings Before and After HPHT Exposure[a]

	average T_g values in °C		
	EN-GPTMS	EN-EPDMS	neat EN[10]
before HPHT exposure (unexposed)	157 ± 3	158 ± 2	155 ± 3
gas-exposed zone (GP)	157 ± 4	157 ± 3	152 ± 4
HC–GP zone	156 ± 2	157 ± 3	135 ± 2
seawater-exposed zone (SW)	155 ± 3	152 ± 2	137 ± 2

[a]DSC measurements were conducted at two different areas of each zone for the two hybrid coatings. For comparison, the average glass transition temperatures for neat EN, reported in ref. 10, are also shown here.

The average T_g value at the gas-exposed zone for both EN-GPTMS and EN-EPDMS was measured to be 157 ± 3 °C, identical to the unexposed samples. The negligible changes in the T_g depression at the gas phase-exposed zone inferred that the high-pressure N_2 and CO_2 individually had no adverse effect on either of the hybrid coatings. The incorporation of long-chain EPDMS and short-chain GPTMS increased the cross-linking further (a higher initial T_g value) when compared to neat EN coatings (T_g of 152 ± 4)[10] and maintained excellent resistance to gas diffusion at HPHT.

The hydrocarbon-exposed zone, where the softening of the neat EN networks, due to para-xylene interactions, was reported[10] is of utmost importance in the present study. In contrast to the softening effect that lowered the T_g at the hydrocarbon exposed zone of neat EN by 20 °C,[10] the addition of the siloxane backbone into the EN network resisted the nonpolar *para*-xylene interaction significantly. The average T_g value at the hydrocarbon-exposed zone was measured to be 156 ± 2 and 157 ± 3 °C for EN-GPTMS and EN-EPDMS, respectively. The chemical inertness of the polar Si–O bond in the siloxane backbone, with a stronger bond energy (≈106 kcal/mol) compared to C–C (≈80 kcal/mol) and C–O bonds (≈80 to 86 kcal/mol) of the organic epoxy network, was superior reportedly because of the depressed basicity of oxygen in the siloxane linkages[28,29] compared to that of its carbon analogue. This depressed basicity arises from the partial delocalization of the oxygen atoms lone pair onto the adjacent silicon atom, reducing its reactivity. Consequently, the Si–O

https://doi.org/10.1021/acsomega.4c02986
ACS Omega 2024, 9, 30675–30684

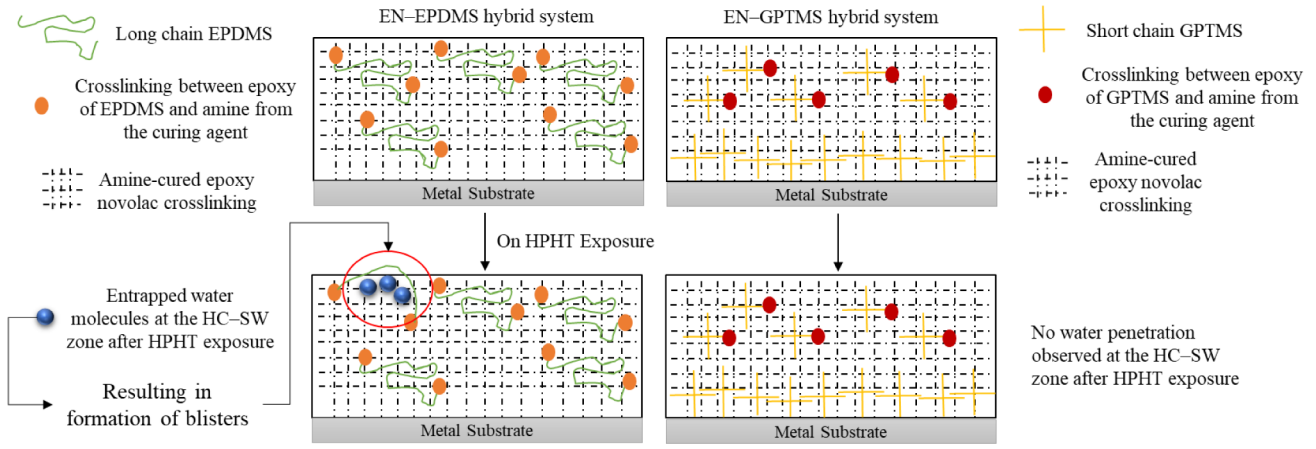

Figure 11. A schematic illustration of EN-EPDMS and EN-GPTMS cross-linking before and after HPHT exposure. The long and flexible chain of EN-EPDMS displays entrapped water molecules at the HC−SW zone, resulting in the formation of unburst blisters. Conversely, the short-chain in EN-GPTMS cross-linked structure shows no change upon exposure to HPHT.

bond exhibits a greater resistance to nucleophilic attacks and other chemical reactions, leading to enhanced stability and durability in various applications. Furthermore, the weak basicity of the Si−O bond was attributed to the p−d dative (p → d) π bonding initially[30] and later elaborated by a model involving hyper conjugative interaction between Si bonding hybrids and antibonding σ^* orbitals.[31−33] A detailed study by Weinhold[29] and West[33] proved that these vicinal hyperconjugative interactions of the siloxane network have profound effects on bond dissociation energies as well as on the related solvent and thermochemical stabilities. In the present study, both the long-chain EPDMS and short-chain GPTMS, due to their siloxane backbone, promote the essential chemical inertness that strongly distinguishes siloxanes from the more reactive ethers of neat EN coatings at HPHT.

For EN-EPDMS, the effectiveness against *para*-xylene, due to the incorporation of a dimethylsiloxane backbone, may also result from the lowered interfacial tensions at the surface. After curing, a more significant microphase separation on the EN-EPDMS surface (as seen in Figures 8 and 9) is a testament that some part of the dimethylsiloxane long chain oriented to the coating surface because of its low surface tension and a certain incompatibility.[29] Although the water contact angles and surface tensions of the present hybrid coatings were not measured, the introduction of dimethylsiloxane backbone leads to surface tension interactions of the nonpolar or Lifshitz−van der Waals (LW) type in the EN-EPDMS coatings.[34] According to the laws for interfacial tensions,[35] the incorporation of EPDMS provides a distinct repellent property to the EN-EPDMS surface compared to the neat EN coating, reducing and delaying the *para*-xylene interaction significantly at HPHT. In the case of EN-GPTMS, the presence of dimethyl groups at the surface is expected to be of low significance; nevertheless, it is noteworthy that the (p → d) π bonding in the siloxane network has been reported to weaken the intermolecular interaction lowering the surface tension.[36] Consequently, no significant change in the T_g values is strong evidence that both hybrid networks resist the hydrocarbon-associated softening effect.

In the case of seawater-exposed zones, it was noteworthy to examine the effect of seawater interactions on both hybrid coatings after HPHT exposure. The only change in the average T_g depression for both EN-GPTMS and EN-EPDMS was at their seawater-exposed zone, measuring a slightly lower value of 155 ± 3 °C and 152 ± 2 °C, respectively. The EN-GPTMS coating remained unaffected, confirming that a combination of high-pressure CO_2 conditions and seawater has no substantial effects on the cross-linking. In the case of neat EN, substantial blister formation at the seawater exposed area[10] was now defect-free for the EN-GPTMS coating as a consequence of the donor−acceptor (p → d) π interaction of the Si−O bond and the silanols bonding with the metal substrate. The resultant (p → d) π conjugation shifts the electron density of the O atom toward the Si atom, making it almost impossible for the oxygen to form a hydrogen bond with the adsorbed water molecules. Furthermore, the silanol condensation reaction that involves a reaction with adjacent silanol yielded a multimolecular structure of cross-linked siloxane. The preference of the silane coupling agent for bonding with the inorganic steel substrate over the polymer can be understood through the condensation process of silane silanols at the interface.[37] As these silanols condense with each other, they form a cross-linked siloxane structure. This cross-linked structure comprises multiple layers of siloxane, characterized by a tightly packed arrangement near the inorganic surface and a more diffuse distribution away from it. Thus, the density of this multimolecular structure would be higher toward the metal−coating interface and gradually form a diffuse structure away from the substrate into the bulk of the coating. This "grid" structure facilitates the interpenetration or diffusion of organic coatings into the siloxane structure, enabling powerful adhesive forces to become part of the bonding mechanism. It is this bonding mechanism where the siloxane multilayer structure in the coating bulk permits the organic epoxy novolac chains to interpenetrate. Consequently, the novolac chains generate the electrostatic forces of interpenetration that impart a much-needed strong adhesive force.[37]

Additionally, the silanol bonds of the GPTMS forming hydrogen bonds to the metal substrate (covalent bonds) lead to one of the strongest interfacial bonds, suggesting that if at all a failure was to be observed, it would be cohesive rather than adhesive. At the same time, it is worth mentioning that the silanols need not form water-resistant "oxane" (Si−O−metal) bonds with the substrate.[38] The covalent siloxane bonds ultimately may hydrolyze.[38] This hydrolysis acts as the origin point for the hydroxyl groups as centers of adsorption for water

https://doi.org/10.1021/acsomega.4c02986
ACS Omega 2024, 9, 30675−30684

molecules. In conclusion, by utilizing short-chain silane (GPTMS) chemistry at HPHT, a significantly delayed interaction with water, even in extreme HPHT conditions, due to the high activation energy (≈23.6 kcal/mol) of Si−O bonds by water, was achieved. Moreover, the hydrocarbon seawater interface (HC−SW zone), where the underfilm corrosion was detected for the neat EN system, remained intact eliminating the diffusion of seawater ions and CO_2 gas.

On the other hand, the EN-EPDMS coating showed the highest T_g depression (±6 °C) at its seawater-exposed zone, but the surface was relatively defect-free and intact. However, the formation of blisters was distinctively toward the hydrocarbon−seawater (HC−SW) interface for EN-EPDMS. The HC−SW zone is the same area reported to experience a synergistic effect of higher water penetrations due to a phase change gradient, increasing the high-pressure CO_2 concentration.[10] Attention should be paid to the long-chain siloxane backbone of the EN-EPDMS coating. Although the dimethylsiloxane backbone's hydrophobicity and the stable siloxane networks show good resistance to water penetration, its chain length influences the internal chain flexibility, increasing the network's fractional free volume. In addition, it is reportedly the most flexible polymeric chain known, both in the dynamic sense and in the equilibrium sense.[39−41] Such flexibility, as an attribute, has a high probability of promoting water molecule entrapment, especially under high-pressure conditions, as illustrated in Figure 11. Additionally, the rapid gas decompression (RGD) in the HPHT domain, which is the rapid depressurization to ambient, further aids in the formation of large unburst blisters, owing to the long and flexible siloxane backbone. The dynamic flexibility of a long-chain siloxane is another reason why the permeability of gases is at its highest for siloxanes compared to other elastomeric materials because it forms a high diffusion rate pathway for the penetrants.[42,43]

It is important to mention that ENEPDMS functions more as a copolymer rather than an adhesion promoter. Unlike GPTMS, which possesses specific functional groups tailored for enhancing the adhesion, EPDMS lacks such adhesive functionalities. Consequently, although EPDMS may demonstrate superior performance in certain aspects, such as elevating the T_g of the coating, its impact on the adhesion of the EN-EPDMS coating is deemed negligible.

Furthermore, the biased affinity of CO_2 present in the HPHT gas phase is significantly higher for a long siloxane chain compared with other gases. Studies attributed this to the ether oxygen moieties in the siloxane, which are polar, favoring the solubility of quadrupolar CO_2.[44−46] Consequently, utilizing a long siloxane chain is critical for HPHT conditions, since high-pressure conditions and the presence of CO_2 in the gas phase are dominant parameters adversely affecting the EN-EPDMS hybrid coatings.

The findings from the present study demonstrate that the CO_2 diffusivity and water penetration scaled with the specific free volume of the siloxane network. Incorporation of the flexible and long-chain siloxane backbone (EPDMS) increased the openness (free volume) in contrast to the short-chained and rigid structure of silane (GPTMS). Owing to its flexible backbone, the long-chained EPDMS proved detrimental and substantiated the physical defects like blisters for HPHT applications.

4. CONCLUSIONS

To obtain superior performance for multiphase HPHT conditions, a long-chain (EPDMS) and a short-chain (GPTMS) silicon derivative, respectively, were incorporated into an amine-cured epoxy novolac resin (EN). After curing, a microphase separation on the surface of both the hybrid coatings, which played no role in the coating degradations at HPHT, was observed. The HPHT gas phase, constituting a mixture of high-pressure CO_2 and N_2, showed no adverse effect on either hybrid networks. Due to the presence of chemically inert and thermally stable siloxane structures in the silicone-modified EN coatings, the previously reported softening effect at the hydrocarbon exposed zone was eliminated. Lastly, the seawater-exposed zone remained intact and defect-free for both EN-EPDMS and EN-GPTMS coatings. However, the entrapment of water molecules at the hydrocarbon−seawater interface, attributed to the long chain length and high flexibility of the EN-EPDMS coating, was identified as a significant drawback. In contrast, the short-chain GPTMS at the same interface exhibited a defect-free surface, establishing its superiority over EN-EPDMS as a more favorable choice for HPHT applications.

■ ASSOCIATED CONTENT

Supporting Information

The Supporting Information is available free of charge at https://pubs.acs.org/doi/10.1021/acsomega.4c02986.

Differential scanning calorimetry (DSC) analysis measuring the average glass transition temperatures (T_g) across the different zones for the coatings before and after HPHT exposure (PDF)

■ AUTHOR INFORMATION

Corresponding Authors

Narayanan Rajagopalan − *The Hempel Foundation Coatings Science and Technology Centre (CoaST), Department of Chemical Engineering, Technical University of Denmark (DTU), Kongens Lyngby 2800, Denmark*; orcid.org/0000-0003-3802-0851; Email: naraj@kt.dtu.dk

Søren Kiil − *The Hempel Foundation Coatings Science and Technology Centre (CoaST), Department of Chemical Engineering, Technical University of Denmark (DTU), Kongens Lyngby 2800, Denmark*; Email: sk@kt.dtu.dk

Authors

Mads Olsen − *The Hempel Foundation Coatings Science and Technology Centre (CoaST), Department of Chemical Engineering, Technical University of Denmark (DTU), Kongens Lyngby 2800, Denmark*

Toke Skaarup Larsen − *The Hempel Foundation Coatings Science and Technology Centre (CoaST), Department of Chemical Engineering, Technical University of Denmark (DTU), Kongens Lyngby 2800, Denmark*

Tine Jensen Fjælberg − *The Hempel Foundation Coatings Science and Technology Centre (CoaST), Department of Chemical Engineering, Technical University of Denmark (DTU), Kongens Lyngby 2800, Denmark*

Claus Erik Weinell − *The Hempel Foundation Coatings Science and Technology Centre (CoaST), Department of Chemical Engineering, Technical University of Denmark (DTU), Kongens Lyngby 2800, Denmark*

Complete contact information is available at:

https://doi.org/10.1021/acsomega.4c02986
ACS Omega 2024, 9, 30675−30684

https://pubs.acs.org/10.1021/acsomega.4c02986

Notes

The authors declare no competing financial interest.

■ ACKNOWLEDGMENTS

Financial support from the Hempel Foundation to CoaST (The Hempel Foundation Coatings Science & Technology Centre) is gratefully acknowledged.

■ ABBREVIATIONS

ATR-FTIR, attenuated total reflectance-Fourier transform infrared; DEAPA, 3-(diethylamino)propylamine; DFT, dry film thickness; DM, digital microscopy; DSC, differential scanning calorimetry; EDX, energy dispersive X-ray; EPDMS, epoxy-terminated polydimethylsiloxane; EN, amine-cured epoxy novolac coating; GP, gas phase; GPTMS, 3-glycidyloxypropyltrimethoxysilane; HC, hydrocarbon phase; HPHT, high-pressure high-temperature; MXDA, *m*-xylylenediamine; PDMS, polydimethylsiloxane; RGD, rapid gas decompression; SEM, scanning electron microscopy; SW, seawater phase

■ SYMBOLS

T_g, glass transition temperature

■ REFERENCES

(1) Shadravan, A.; Amani, M. HPHT 101: What Every Engineer or Geoscientist Should Know About High Pressure High Temperature Wells. In *SPE Kuwait International Petroleum Conference and Exhibition*. Society of Petroleum Engineers, 2012.

(2) Skeels, H. B. API 17TR8 - HPHT Design Guideline for Subsea Equipment. In *Offshore Technology Conference*, OnePetro, 2014. Paper Number: OTC-25376-MS.

(3) Singh, A.; Lin, Y.; Ebenso, E. E.; Liu, W.; Huang, B. Determination of Corrosion Inhibition Efficiency Using HPHT Autoclave by Gingko Biloba on Carbon Steels in 3.5% NaCl Solution Saturated with CO_2. *Int. J. Electrochem. Sci.* **2014**, *9*, 5993−6005.

(4) Elgaddafi, R.; Ahmed, R.; Hassani, S.; Shah, S.; Osisanya, S. O. Corrosion of C110 Carbon Steel in High-pressure Aqueous Environment with Mixed Hydrocarbon and CO2 Gas. *J. Pet. Sci. Eng.* **2016**, *146*, 777−787.

(5) Pu, F.; Philip, R. P.; Zhenxi, L.; Guangguo, Y. Geochemical Characteristics of Aromatic Hydrocarbons of Crude Oils And Source Rocks From Different Sedimentary Environments. *Org. Geochem.* **1990**, *16* (1−3), 427−435.

(6) Kashefi, K.; Chapoy, A.; Bell, K.; Tohidi, B. Viscosity of Binary and Multicomponent Hydrocarbon Fluids at High Pressure and High Temperature Conditions: Measurements and Predictions. *J. Pet. Sci. Eng.* **2013**, *112*, 153−160.

(7) Hua, R.; Jianzhong, S.; Binjie, W.; Qiyun, Z. Synthesis and Curing Properties of a Novel Novolac Curing Agent Containing Naphthyl and Dicyclopentadiene Moieties. *Chin. J. Chem. Eng.* **2007**, *15* (1), 127−131.

(8) Pham, H. Q.; Marks, M. J. Epoxy Resins. In *Ullmann's Encyclopedia of Industrial Chemistry*; Wiley-VCH, 2000.

(9) Rajagopalan, N.; Weinell, C. E.; Dam-Johansen, K.; Kiil, S. Degradation Mechanisms of Amine-Cured Epoxy Novolac and Bisphenol F Resins Under Conditions of High Pressures and High Temperatures. *Prog. Org. Coat.* **2021**, *156*, 106268.

(10) Rajagopalan, N.; Weinell, C. E.; Dam-Johansen, K.; Kiil, S. Influence of CO2 at HPHT Conditions on the Properties and Failures of an Amine-Cured Epoxy Novolac Coating. *Ind. Eng. Chem. Res.* **2021**, *60* (41), 14768−14778.

(11) Ren, H.; Qu, Y.; Zhao, S. Reinforcement of Styrene-Butadiene Rubber with Silica Modified by Silane Coupling Agents: Experimental and Theoretical Chemistry Study. *Chin. J. Chem. Eng.* **2006**, *14* (1), 93−98.

(12) Witucki, G. L. A Silane Primer: Chemistry and Applications of Alkoxy Silanes. *J. Coat. Technol.* **1993**, *65*, 57−57.

(13) Pape, P. G. Adhesion Promoters: Silane Coupling Agents. In *Applied plastics engineering handbook*; William Andrew Publishing, 2011; pp. 503517.

(14) Mark, J. E. Overview of Siloxane Polymers. In *Silicones and Silicone-Modified Materials, Chapter 1*, Clarson, S. J.; Fitzgerald, J. J.; Owen, M. J.; Smith, S. D. Eds ACS Publications, 2000; pp. 110.

(15) Shit, S. C.; Shah, P. A Review on Silicone Rubber. *Natl. Acad. Sci. Lett.* **2013**, *36* (4), 355−365.

(16) Amin, M.; Akbar, M.; Amin, S. Hydrophobicity of Silicone Rubber Used for Outdoor Insulation (an Overview). *Rev. Adv. Mater. Sci.* **2007**, *16*, 10−26.

(17) Ahmad, S.; Gupta, A. P.; Sharmin, E.; Alam, M.; Pandey, S. K. Synthesis, Characterization and Development of High Performance Siloxane-modified Epoxy Paints. *Prog. Org. Coat.* **2005**, *54* (3), 248−255.

(18) Klopffer, M. H.; Flaconneche, B. Transport Properties of Gases In Polymers: Bibliographic Review. *Oil Gas Sci. Technol.* **2001**, *56* (3), 223−244.

(19) Buyl, F. Silicone Sealants and Structural Adhesives. *Int. J. Adhes. Adhes.* **2001**, *21* (5), 411−422.

(20) Wang, P.; Schaefer, D. W. Why Does Silane Enhance The Protective Properties of Epoxy Films? *Langmuir* **2008**, *24* (23), 13496−13501.

(21) Mazurek, M. H. *Silicones, comprehensive organometallic chemistry III, from fundamentals to applications*; Elsevier: Amsterdam, 2007; pp. 651697.

(22) Southwart, D. W. Comparison of Bound Rubber and Swelling in Silicone Rubber/Silica Mixes and in Silicone Rubber Vulcanizates. *Polymer* **1976**, *17* (2), 47−152.

(23) Fedrizzi, L.; Andreatta, F.; Paussa, L.; Deflorian, F.; Maschio, S. Heat Exchangers Corrosion Protection by Using Organic Coatings. *Prog. Org. Coat.* **2008**, *63* (3), 299−306.

(24) Kr, V. K.; Sundareswaran, V. The Effect of Thermal Barrier Coatings on Diesel Engine Performance of PZT Loaded Cyanate Modified Epoxy Coated Combustion Chamber. *JJMIE* **2011**, *5* (5), 403−406.

(25) Seiersten, M.; Kongshaug, K. O.Materials Selection for Capture, Compression, Transport and Injection of CO2*Carbondioxide Capture For Storage In Deep Geologic Formations*Elsevier2005937

(26) Flowserve. *Oil And Gas Upstream and Pipeline*, 2021. https://www.flowserve.com/sites/default/files/2016-07/fpd-3-ea4_0.pdf.

(27) Majumdar, P.; Webster, D. C. Surface Microtopography in Siloxane−Polyurethane Thermosets: The Influence of Siloxane and Extent of Reaction. *Polymer* **2007**, *48* (26), 7499−7509.

(28) Weinhold, F.; West, R. The Nature of The Silicon−Oxygen Bond. *Organometallics* **2011**, *30* (21), 5815−5824.

(29) Weinhold, F.; West, R. Hyperconjugative Interactions in Permethylated Siloxanes and Ethers: The Nature of The Si-o Bond. *J. Am. Chem. Soc.* **2013**, *135* (15), 5762−5767.

(30) Craig, D. P.; Maccoll, A.; Nyholm, R. S.; Orgel, L. E.; Sutton, L. E. Chemical Bonds Involving d-Orbitals. Part I. *J. Chem. Soc.* **1954**, 332−353.

(31) Shambayati, S.; Schreiber, S. L.; Blake, J. F.; Wierschke, S. G.; Jorgensen, W. L. Structure and Basicity of Silyl Ethers: A Crystallographic and Ab Initio Inquiry Into The Nature of Silicon-Oxygen Interactions. *J. Am. Chem. Soc.* **1990**, *112* (2), 697−703.

(32) Pitt, C. G. Hyperconjugation and Its Role in-group IV Chemistry. *J. Organomet. Chem.* **1973**, *61*, 49−70.

(33) West, R.; Wilson, L. S.; Powell, D. L. Basicity of Siloxanes, Alkoxysilanes and Ethers Toward Hydrogen Bonding. *J. Organomet. Chem.* **1979**, *178* (1), 5−9.

(34) Holberg, S.; Bischoff, C. Application of a Repellent Urea−siloxane Hybrid Coating in the Oil Industry. *Prog. Org. Coat.* **2014**, *77* (10), 1591−1595.

https://doi.org/10.1021/acsomega.4c02986
ACS Omega 2024, 9, 30675−30684

(35) Van Oss, C. J.; Good, R. J.; Chaudhury, M. K. Additive and Nonadditive Surface Tension Components and the Interpretation of Contact Angles. *Langmuir* **1988**, *4* (4), 884−891.
(36) Voronkov, M. G.; Yuzhelevskii, Y. A.; Mileshkevich, V. P. The Siloxane Bond and its Influence on the Structure and Physical Properties of Organosilicon Compounds. *Russ. Chem. Rev.* **1975**, *44* (4), 355.
(37) Pape, P. G. Adhesion Promoters: Silane Coupling Agents. In *Applied plastics engineering handbook*; William Andrew Publishing, 2011; pp. 503517.
(38) Laskorin, B. N.; Strelko, V. V.; Strazhesko, D. N.; Denisov, V. I. *Sorbents based on silica gel in radiochemistry*; Atomizdat: Moscow, 1977.
(39) Flory, P. J.; Volkenstein, M. Statistical Mechanics of Chain Molecules. *Biopolymers* **1969**, *8* (5), 699−700.
(40) Mark, J. E.; Eisenberg, A.; Graessley, W. W.; Mandelkern, L.; Koenig, J. L. The rubber elastic state. In *Physical properties of polymers*; Cambridge University Press, 2004; pp. 3371.
(41) Bahar, I.; Zuniga, I.; Dodge, R.; Mattice, W. L. Conformational Statistics of Poly (Dimethylsiloxane). 1. Probability Distribution of Rotational Isomers from Molecular Dynamics Simulations. *Macromolecules* **1991**, *24* (10), 2986−2992.
(42) Freeman, B.; Yampolskii, Y.; Pinnau, I. *Materials science of membranes for gas and vapor separation*; John Wiley & Sons, 2006.
(43) Reijerkerk, S. R.; Knoef, M. H.; Nijmeijer, K.; Wessling, M. Poly (Ethylene Glycol) and Poly (Dimethyl Siloxane): Combining their Advantages Into Efficient Co2 Gas Separation Membranes. *J. Membr. Sci.* **2010**, *352* (1−2), 126−135.
(44) Bondar, V. I.; Freeman, B. D.; Pinnau, I. Gas Sorption and Characterization of poly (ether-b-amide) Segmented Block Copolymers. *J. Polym. Sci., Part B: Polym. Phys.* **1999**, *37* (17), 2463−2475.
(45) Bondar, V. I.; Freeman, B. D.; Pinnau, I. Gas Transport Properties of Poly (Ether-B-Amide) Segmented Block Copolymers. *J. Polym. Sci., Part B: Polym. Phys.* **2000**, *38* (15), 2051−2062.
(46) Lin, H.; Freeman, B. D. Materials Selection Guidelines for Membranes that Remove CO2 from Gas Mixtures. *J. Mol. Struct.* **2005**, *739* (1−3), 57−74.

https://doi.org/10.1021/acsomega.4c02986
ACS Omega 2024, 9, 30675−30684